Since January 2020 Elsevier has created a COVID-19 resource centre with free information in English and Mandarin on the novel coronavirus COVID-19. The COVID-19 resource centre is hosted on Elsevier Connect, the company's public news and information website.

Talanta 251 (2023) 123783

Contents lists available at ScienceDirect

Talanta

journal homepage: www.elsevier.com/locate/talanta

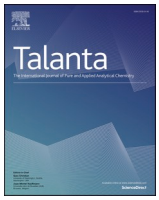

Electrochemical paper-based antigen sensing platform using plant-derived monoclonal antibody for detecting SARS-CoV-2

Jutamas Jaewjaroenwattana [a], Waranyoo Phoolcharoen [b], Ekawat Pasomsub [c], Prinjaporn Teengam [a,**], Orawon Chailapakul [a,*]

[a] Electrochemistry and Optical Spectroscopy Center of Excellence, Department of Chemistry, Faculty of Science, Chulalongkorn University, Pathumwan, Bangkok, 10330, Thailand
[b] Department of Pharmacognosy and Pharmaceutical Botany, Faculty of Pharmaceutical Sciences, Center of Excellence in Plant-produced Pharmaceuticals, Chulalongkorn University, Pathumwan, Bangkok, 10330, Thailand
[c] Division of Virology, Department of Pathology, Faculty of Medicine Ramathibodi Hospital, Mahidol University, Bangkok, Thailand

ARTICLE INFO

Keywords:
SARS-CoV-2
Plant-based antibody
Paper-based electrochemical immunosensor
Differential pulse voltammetry
Point-of-care

ABSTRACT

The current approaches of diagnostic platforms for detecting SARS-CoV-2 infections mostly relied on adapting the existing technology. In this work, a simple and low-cost electrochemical sensing platform for detecting SARS-CoV-2 antigen was established. The proposed sensor combined the innovative disposable paper-based immunosensor and cost-effective plant-based anti-SARS-CoV-2 monoclonal antibody CR3022, expressed in *Nicotiana benthamiana*. The cellulose nanocrystal was modified on screen-printed graphene electrode to provide the abundant COOH functional groups on electrode surface, leading to the high ability for antibody immobilization. The quantification of the presence receptor binding domain (RBD) spike protein of SARS-CoV-2 was performed using differential pulse voltammetry by monitoring the changing current of $[Fe(CN)_6]^{3-/4-}$ redox solution. The current change of $[Fe(CN)_6]^{3-/4-}$ before and after the presence of target RBD could be clearly distinguished, providing a linear relationship with RBD concentration in the range from 0.1 pg/mL to 500 ng/mL with the minimum limit of detection of 2.0 fg/mL. The proposed platform was successfully applied to detect RBD in nasopharyngeal swab samples with satisfactory results. Furthermore, the paper-based immunosensor was extended to quantify the RBD level in spiked saliva samples, demonstrating the broadly applicability of this system. This electrochemical paper-based immunosensor has the potential to be employed as a point-of-care testing for COVID-19 diagnosis.

1. Introduction

The pandemic of Coronavirus disease (COVID-19) caused by Severe Acute Respiratory Syndrome Coronavirus 2 (SARS-CoV-2) has become a major public health problem worldwide. World Health Organization (WHO) reported that 518 million populations have been infected with over 6.3 million deaths as of June 2022 [1]. Even though the vaccines have been currently developed for preventing infection, the number of newly infected patient still hardly reduces due to mutations of the virus [2,3]. The outbreak has therefore begun to enable diagnostic assays for screening and preventing the spread of the disease. Current diagnostic methods have solely relied on the nucleic acid amplification technologies, such as real time - polymerase chain reaction (RT-PCR) [4–6] and Loop mediated isothermal amplification (LAMP) [7–9]. Nevertheless, these methods have merits, such as they require expensive instruments and sophisticated operation steps which are the key bottlenecks in testing that dramatically increases cost and assay time from sample-to-answer. Therefore, more recent efforts have focused on serological assays to determine prior infection [10–12]. Enzyme-linked immunosorbent assay (ELISA) represents the gold standard method for serological testing, which is expensive and must perform in laboratory setting [13,14]. Lateral flow immunoassays (LFAs) have been developed to serve as a point-of-care (POC) tool since they are easy to use and provide qualitative (yes/no) or semi-quantitative results [15,16]. However, LFAs are relatively low sensitive, making them prone to false positive and/or negative results [17]. Thus, significant improvements of

* Corresponding author.
** Corresponding author.
E-mail addresses: p.teengam@hotmail.com (P. Teengam), corawon@chula.ac.th (O. Chailapakul).

https://doi.org/10.1016/j.talanta.2022.123783
Received 9 June 2022; Received in revised form 20 July 2022; Accepted 24 July 2022
Available online 7 August 2022

COVID-19 testing are needed to replace laboratory testing as well as provide a rapid and sensitive diagnostic information to patients and health care provider.

Electrochemical immunosensors have been continuously developed and applied in various biosensing applications [18–20] as they offer the advantages of high sensitivity, simplicity and ability in quantitative analysis. However, traditionally electrochemical detection relied on the bulky instruments, limiting their potential for point-of-need applications. The electrochemical paper-based analytical devices (ePADs) [21–25] were introduced to address the challenge for developing miniaturized system. ePADS have garnered significant interest to utilize as an alternative device design for immunoassay because they exhibit remarkable advantages, including easy-to-use, inexpensive, portability and disposability. However, to achieve a highly sensitive diagnostic platform, the major obstruction is the limited area as part of the micro-scale electrode, leading to even lower limit of detection (LOD).

Cellulose nanomaterials (CNs), especially cellulose nanofiber (CNF) and cellulose nanocrystal (CNC) are the new generation materials that have currently gained growing interest. CNs possess the attractive properties including abundance of functional groups, high aspect ratio, strong mechanical properties and biocompatibility. Importantly, CNs contained the abundant COOH and/or OH functional groups on the structure, allowing various functionalizations via chemical reactions. These excellent characteristics enable them to be widely applied in chemo/biosensors applications [26,27].

Regarding the immunoassay, antibody is the key factor to limit the sensitivity and selectivity of the method. Most commercially available antibodies are produced in mammalian cells which still have some limitations, such as high production costs and complication processes. Moreover, mammalian-produced antibody could lead potentially humans to infections [28,29]. Recently, plants are being exploited as a new alternative host for antibody production, especially during unexpected or emergency situations that cannot be solved by existing systems. Plant-based antibody provides many advantages, such as low-cost, eco-friendly and rapid production [30]. In 2020, Rattanapisit and co-workers proposed the use of a temporary expression method to produce the receptor binding domain (RBD) spike protein of SARS-CoV-2 and monoclonal antibody (mAb) CR3022 in *Nicotiana benthamiana* [31]. This plant-produced RBD and mAb CR3022 illustrated a specific binding toward SARS-CoV-2. Interestingly, this plant-based antibody has capability to apply in immunological sensing applications.

Here, we reported a paper-based electrochemical immunosensor using CNC-modified electrode in combination with novel plant-based monoclonal antibody that was used as a capture antibody for detecting RBD of SARS-CoV-2 spike protein for the first time. Differential pulse voltammetry (DPV) was used to quantify the RBD level by measuring the current response of $[Fe(CN)_6]^{3-/4-}$ redox solution. This immunosensor was successfully applied for detection of SARS-CoV-2 RBD in nasopharyngeal swab samples and can be extended to saliva sample, which exhibits good analytical performance, is easy to use and low-cost for SARS-CoV-2 diagnosis.

2. Materials and methods

2.1. Chemicals and apparatus

All reagents used are analytical reagent grade. Cellulose nanocrystal with carboxylic group (CNC–COOH) was purchased from cellulose lab (Fredericton, Canada). mAb CR3022 (GenBank accession numbers: DQ168569.1 and DQ168570.1) and RBD of SARS-CoV-2 spike protein (GenBank accession number: YP_009724390.1; F318–C617) were obtained from Baiya Phytopharm Co., Ltd. (Bangkok, Thailand). Potassium hexacyanoferrate (III) ($K_3Fe(CN)_6$), phosphate buffer saline (PBS) pH 7.4, 1-ethyl-3-(3-dimethylaminopropyl) carbodiimide (EDC), N-hydroxysulfosuccinimide (sulfo-NHS), skim milk (SKI) and human serum albumin (HSA) were purchased from Sigma-Aldrich (Missouri, USA). Potassium nitrate (KNO_3), L-(+) -ascorbic acid and D-(+)- glucose anhydrous were purchased from Carlo Erba (Barcelona, Spain). Artificial saliva was obtained from (Sigma-Aldrich). All aqueous solutions were prepared using ultra-purified Milli-Q water ($R \geq 18.2\ M\Omega\ cm^{-1}$ at 25 °C) from Merck Millipore (Millipore Bedford, USA).

Graphene and silver/silver chloride (Ag/AgCl) inks were purchased from Serve Science Co., Ltd. (Bangkok, Thailand). Filter paper grade no. 1 was obtained from Whatman international Ltd, (St Louis, USA). The screen-printed pattern was designed using Adobe Illustrator and the screen-printing block was made by Chaiyaboon Co. Ltd, (Bangkok, Thailand). The hydrophobic and hydrophilic area on ePADs were created by a wax printer (Xerox Color Qube model 8570, Japan). Field emission scanning electron microscopy (FE-SEM) (7610F at 5 kV) was used to confirm the success of electrode modification. All electrochemical measurements were performed using PalmSens 4 potentiostat (PalmSens Bv, Netherlands). The electrochemical impedance spectroscopy (EIS) was carried out in the frequency range of 100 kHz to 0.01 Hz and AC potential of 0.25 V. (vs Ag/AgCl). Cyclic votammetry was performed from −0.3 to 0.6 V with scan rate of 0.1 V/s. DPV was used throughout the experiment with the conditions are as follows: potential range of −0.3 to 0.7 V. (vs Ag/AgCl), step potential of 0.01 V, pulse potential of 0.05 V and scan rate of 0.05 V/s.

2.2. Production of monoclonal plant-based antibody (CR3022)

The anti-SARS-CoV-2 mAb CR3022 was prepared using plant transient expression systems as previously described [31]. Briefly, the coding mAb CR3022 gene fragments located in the regions of the variable heavy chain (V_H) and variable light chain (V_L) were codon-optimized to express in *N. benthamiana*. The V_H and V_L were fused with human IgG1 constant heavy chain (C_H) and constant light chain (C_L) regions, respectively. The expression cassettes pBY2e-CR3022 HC and pBY2e-CR3022 LC was created by cloning the full coding sequences of CR3022 HC and LC into a geminiviral vector (pBY2e) using a three fragment ligation [29]. The obtained expression vectors were then transformed into *Agrobacterium tumefaciens* strain GV3101 by electroporation. Next, recombinant *Agrobacterium* containing pBY2e-CR3022 HC and pBY2e-CR3022 LC were pelleted and resuspended in infiltration buffer to an OD_{600} of 0.4 and mixed at a 1:1 ratio prior to vacuum infiltration and infiltrated into the *N. benthamiana* leaves which were grown in a greenhouse with 8 h dark/16 h light cycle at 25 °C for 6–8 weeks. After 3 days, the agroinfiltrated leaves were harvested and extracted proteins in extraction buffer (pH 7.4) [32]. The extracted part was homogenized followed by centrifugation at 15,000 g for 30 min at 4 °C to obtain the crude extract. The recombinant protein in the clarified plant extract was purified by using protein A resin. Finally, the obtained mAb CR3022 was confirmed by SDS-PAGE and Western blot.

2.3. Design and fabrication of paper-based electrochemical immunosensor

The paper-based immunosensor was prepared using filter papers (Whatman No.1). The screen-printed pattern was designed by Adobe Illustrator CS6. A commercial wax printer (ColorQube8580) was used to create hydrophobic areas according to the pattern design. After wax printing, the patterned paper was heated at 150 °C for 1 min to melt the wax and obtain the hydrophobic barrier. Fig. 1 shows the design and operation of paper-based immunosensor. As shown in Fig. 1A, this paper-based immunosensor consists of two parts: the detection and absorbent part. The detection part contains three electrode system, which fabricated by using an in-house screen-printing method. Graphene ink was employed to prepare the working (3 mm i. d.) (WE) and counter (CE) electrodes. Silver/silver chloride (Ag/AgCl) ink was served as the pseudo-reference electrode (RE) and conductive pads. The absorbent part was designed by attaching the absorbent pad to the backside using the double-sided adhesive tape (Fig. 1B). The device was assembled by folding the absorbent part under the detection part to

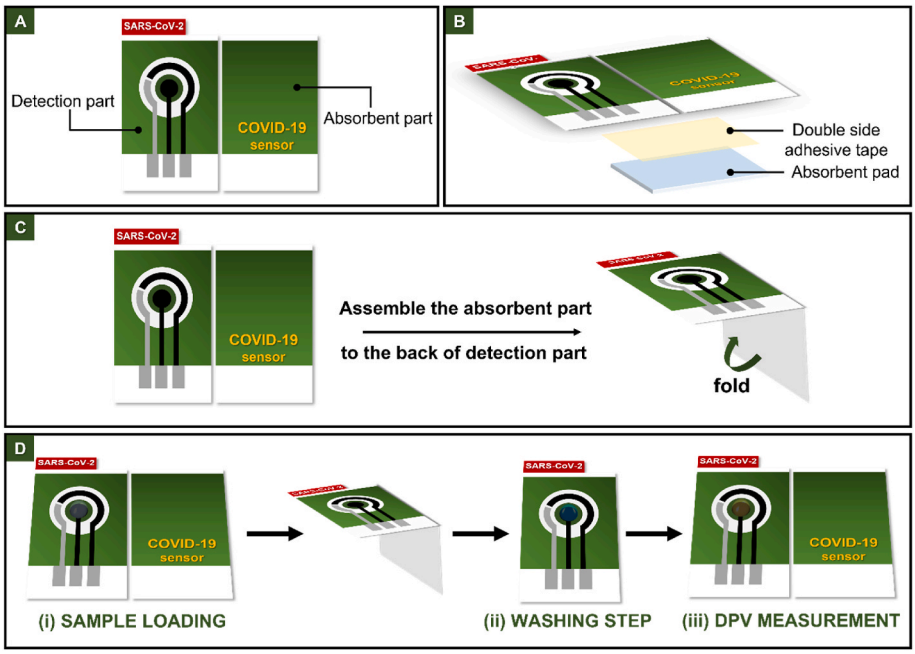

Fig. 1. The design in top view (A), side view (B), the operation (C) and the detection procedure (D) of paper-based electrochemical immunosensor.

utilize the wicking ability of the absorbent pad during the washing step after sample addition (Fig. 1C). The device operational steps were illustrated in Fig. 1D.

2.4. Immobilization of mAb CR3022

For the immobilization step, the mAb CR3022 was covalently immobilized onto working electrode surface. The steps of antibody immobilization were shown in Scheme 1. First, 5 μL of 0.25% CNC solution in Milli-Q water was dropped onto WE to provide the carboxylic group (COOH) on the electrode surface. Then, allowing CNC to dry in an oven at 37 °C for 15 min. Next, 5 μL of EDC/NHS (10 mM/30 mM) solution containing 0.96 mg of EDC and 3.25 mg of sulfo-NHS prepared in PBS pH 7.4 (500 μL) was added onto the CNC-modified electrode surface to act as a coupling agent and incubated at room temperature for 1 h to activate the COOH group, followed by washing with PBS pH 7.4. Then, 1 μg/mL of mAb CR3022 capture antibody (5 μL) was dropped onto the modified electrode surface and incubated in humid condition for 1 h to generate the covalent attachment through the direct conjugation between a carboxylic group (COOH) of CNC and the primary amine groups ($–NH_2$) of the capture antibodies. After that, the Ab/CNC/SPGE electrode was washed twice with PBS pH 7.4 to remove the excess unbound antibodies on WE surface. Next, the electrode surface was blocked with 5 μL of 2% (w/v) skim milk (SKI) solution for 1 h to prevent the nonspecific binding protein. Finally, the SKI/Ab/CNC/SPGE was washed twice with PBS pH 7.4 and stored at 4 °C prior to use.

2.5. Electrochemical measurement

For electrochemical detection, 5 μL of a designated RBD concentration prepared in PBS pH 7.4 was dropped onto electrode surface and incubated in humid condition for 2 h. After incubation, the absorbent part was folded under the detection part (as shown in Fig. 1C), followed by washing all unbonded antigen with PBS pH 7.4. The washed solution could be absorbed due to the wicking property of the absorbent pad. The absorbent part was then unfolded prior to electrochemical detection. All electrochemical measurements were carried out using 5 mM $[Fe(CN)_6]^{3-/4-}$ in 0.1 M KNO_3.

2.6. Real sample analysis

The clinical nasopharyngeal and throat swab samples were obtained

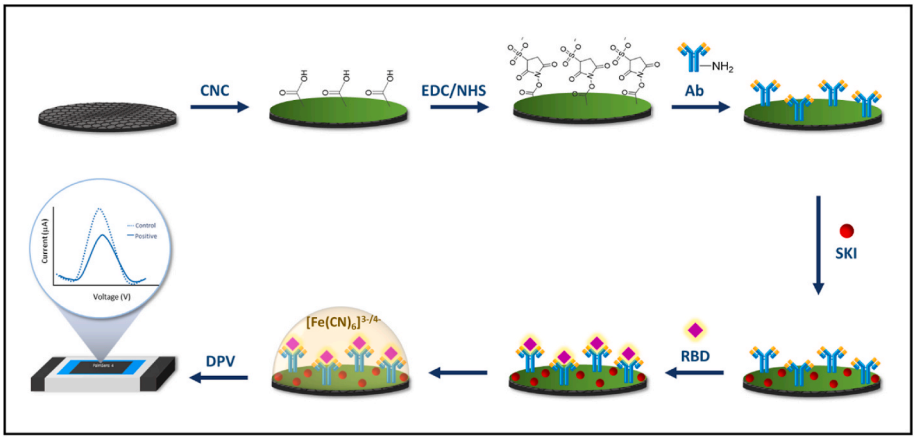

Scheme 1. The process of mAb CR3022 covalent immobilization onto the electrode surface for electrochemical detection of SARS-CoV-2 RBD.

following the protocol approved by the Institutional Review Board, Faculty of Medicine, Ramathibodi Hospital (Certification of approval: COA. MURA2021/879). Written informed consent and ethical approval was obtained for all patients. All samples were collected and stored in viral transport media (VTM) at −80 °C prior to electrochemical measurement using the aforementioned procedure. Finally, the obtained results were validated with those obtained from the standard RT-PCR.

3. Results and discussion

3.1. Surface characterization of CNC modified electrode

To investigate whether the electrode surface was successfully modified with CNC, the surface morphologies of unmodified and modified electrodes were carried out by FE-SEM and laser scanning confocal microscope (LSCM). As shown in Fig. S1A, the unmodified electrode exhibited a rough surface with graphene sheets (panel i). Moreover, the LSCM showed yellow-green areas, indicating the stacked surfaces of graphene sheets with an average roughness of 3.071 μm. After drop casting of CNC, a smooth-like film covering the electrode surface (panel ii) was observed. The LSCM provided the green-blue areas, indicating the low-roughness areas with an average roughness of 2.371 μm. In addition, Fourier-transform infrared spectroscopy (FT-IR) was used to confirm the existence of the carboxylic group on CNC modified electrode surface. The obtained FT-IR spectra of unmodified and modified electrodes were shown in Fig. S1B, all typical bands of CNC including C=O stretching at 1730 cm^{-1}, C–O stretching at 1025 cm^{-1}, C–H stretching at 2945 cm^{-1} and OH stretching at 3350 cm^{-1} were observed. Although, the obtained characteristic bands of the CNC/SPGE were similar to bare SPGE, the characteristic peak of C=O stretching at 1730 cm^{-1}, OH stretching at 3350 cm^{-1} and C–H stretching at 2945 cm^{-1} increased, owing to the presence of CNC. These results confirmed the success of CNC modification on electrode surface.

3.2. Electrochemical characterization

In order to follow electrode modification steps, the electrochemical impedance spectroscopy (EIS) measurement was performed in a stepwise surface modification using 5 mM $[Fe(CN)_6]^{3-/4-}$ in 0.1 M KNO_3. The semicircle diameter of the Nyquist curve represents the electron transfer resistance (R_{ct}), indicating the capability of electron transfer between the electrode surface and redox solution. The R_{ct} increase when insulator molecules were added onto surface of the electrode. The Nyquist plots at different stages of modification process were shown in Fig. 2A. The bare SPGE provided the smallest semicircle with the R_{ct} value of 1.13 kΩ. After modification of CNC (CNC/SPGE), the R_{ct} value increased to 1.71 kΩ due to its semi-insulator property. When Ab was added onto the electrode surface (Ab/CNC/SPGE), the R_{ct} increased to 2.0 kΩ, indicating the success in covalent immobilization of antibodies onto electrode surface. The increment of R_{ct} (3.5 kΩ) was further observed on SKI/Ab/CNC/SPGE due to the steric hindrance of SKI, resulting in a lower accessibility of $[Fe(CN)_6]^{3-/4-}$ to reach the electrode surface [33].

Furthermore, CV was used to verifiy the success of electrode modification by monitoring the current change using 5 mM $[Fe(CN)_6]^{3-/4-}$ in 0.1 M KNO_3. As shown in Fig. 2B, the highest anodic peak current was observed on SPGE (0.108 mA). A decrease in anodic peak current (0.084 mA) was observed after modification of CNC (CNC/SPGE) due to an oxidation of electron transfer affected by the semi-insulator CNC. When the Ab was immobilized onto CNC/SPGE, the anodic current decreased to 0.067 mA indicated that the Ab was successfully immobilized onto electrode surface via covalent reaction. After blocking with SKI (SKI/Ab/CNC/SPGE), the anodic current further decreased to 0.028 mA. These results clearly demonstrated the successful modification of the electrode surface.

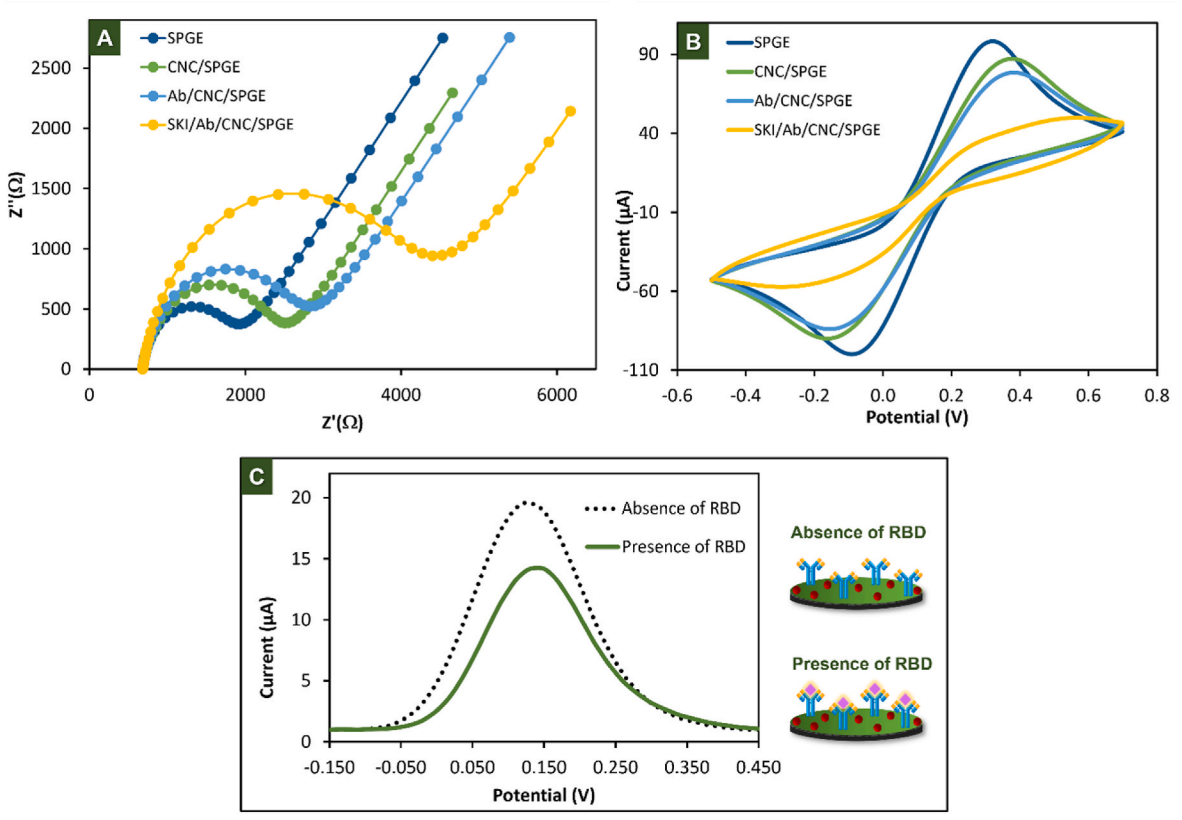

Fig. 2. Characterization of the modified electrodes in a step-by-step by EIS (A), CV (B), and the current response of 5 mM $[Fe(CN)_6]^{3-/4-}$ in the absence and presence of 500 ng/mL of RBD that were performed by DPV (C).

The electrochemical detection of SKI/Ab/CNC/SPGE before and after addition of SARS-CoV-2 spike protein RBD was then investigated using DPV. As displayed in Fig. 2C. In the presence of RBD, a lower electron transfer could be observed due to the shielding of the electrode surface by the immunocomplex, resulting in a remarkable decrease of the current response [34]. This result confirmed the formation of antigen-antibody complex on the electrode surface. All obtained results suggested that the proposed immunosensor can be applied for detecting SARS-CoV-2.

3.3. Optimization of variable parameters

3.3.1. Effect of CNC concentration

The effect of CNC concentration was firstly investigated. The CNC was studied in the concentration range from 0.1 to 0.3% (v/v) using the condition as follows: 1 μg/mL of Ab, 5% (w/v) of SKI, 0.5 μg/mL of RBD and incubation time of 60 min. As shown in Fig. S2A, the change in current response (ΔI) obtained before and after incubation with RBD increased with the increase of CNC concentration. This is due to the enlargement in carboxyl group at the higher concentration of CNC, leading to more sites for Ab immobilization. However, the ΔI value decreased at the CNC concentration above 0.25% which could be explained by the formation of self-assembled CNC as a film layer on the electrode surface that reduced the binding site of Ab immobilization [35]. Therefore, 0.25% (v/v) of CNC concentration was selected for the next studies.

3.3.2. Effect of Ab concentration

The effect of Ab concentration was then optimized in the range of 0.25–1.25 μg/mL using the condition as follows: 0.25% (v/v) of CNC, 5% (w/v) of SKI, 0.5 μg/mL of RBD and incubation time of 60 min. As shown in Fig. S2B, the ΔI increased with the increasing of Ab concentration until it plateaued at the concentration of 1 μg/mL due to an oversaturation of the electrode surface at conditions above this limitation. Additionally, the higher amount of Ab also increased the surface density that hindered the accessibility of more Ab to immobilize onto the electrode surface [36]. Thus, the 1 μg/mL of Ab concentration was selected for further experiments.

3.3.3. Effect of SKI concentration

In this work, SKI was utilized as a surface blocking agent due to its capability to prevent a nonspecific binding and provide the higher ratio of signal/background (S/B) when compared to bovine serum albumin (BSA) [19]. SKI concentration was optimized in the range from 1% to 5% (w/v) using the condition as follows: 0.25% (v/v) of CNC, 1 μg/mL of Ab, 0.5 μg/mL of RBD and incubation time of 60 min. The ΔI obtained before and after incubation with RBD as a function of SKI concentration is displayed in Fig. S2C. It was observed that the ΔI increased with increasing SKI concentration and reached the maximum at 2% (w/v). When the higher SKI concentration was applied, the background signal in the absence of target RBD was also risen, resulting in the decrease of ΔI value. Therefore, 2% (w/v) of SKI concentration was used for further experiments.

3.3.4. Effect of incubation time

The influence of incubation time between the RBD target and Ab immobilized on electrode surface was optimized. The 0.5 μg/mL of RBD was incubated on Ab-modified electrode at different times followed by washing with PBS. As illustrated in Fig. S2D, the ΔI slightly increased with the increasing of incubation time and reached a plateau after 2 h. This result indicated that the increase in incubation time provided the improvement of binding efficiency between Ab and target RBD [37]. However, the electrode surface likely saturated at longer incubation time, resulting in a limited mass transport of redox molecules to access the electrode surface [38]. Therefore, the incubation time of 2 h was selected as an optimal condition.

3.4. Analytical performances of the paper-based immunosensor

The analytical performance of the paper-based electrochemical immunosensor for detecting SARS-CoV-2 was evaluated. As shown in Fig. 3A, the current signal of $[Fe(CN)_6]^{3-/4-}$ decreased as a function of RBD concentrations. Fig. 4B shows that the change in current response (ΔI) calculated from I_{blank}-I_{RBD} (where I_{blank} and I_{RBD} are obtained before and after incubation with RBD) increased with the increasing of RBD concentration. The calibration curve obtained by plotting between ΔI versus logarithmic concentrations (Fig. 3B inset) provided a linear relationship in the range from 0.1 pg/mL to 500 ng/mL with correlation coefficient of 0.9931. The limit of detection (LOD, S/N = 3) and limit of quantification (LOQ, S/N = 10) were calculated to be 2 fg/mL and 8 fg/mL, respectively. The analytical performance of this proposed immunosensor and other previously reported systems for screening of SARS-CoV-2 are compared and summarized as shown in Table S1. The compared results suggested that a significant lower detection limit obtained from our proposed immunosensor. Notably, our paper-based immunosensor combined with the plant-based antibody can be easily and inexpensively prepared compared to the other SAR-CoV-2 biosensors.

3.5. Cross-reactivity

To investigate the cross-reactivity of various virus antigens, the proposed paper-based immunosensor was used to test with different types of human-pathogenic coronaviruses and respiratory viruses, including Recombinant SARS Nucleocapsid (N) Protein (SARS-CoV-1), Recombinant Human Coronavirus MERS Spike Glycoprotein (S1), Recombinant Human Respiratory Syncytial Virus (RSV) Glycoprotein, Recombinant Human Coxsackie Adenovirus Receptor and Influenza as illustrated in Fig. 4. All antigens were prepared at the same concentration of 0.1 ng/mL before incubating onto electrode surface followed by the electrochemical measurement. The percent normalized currents were evaluated from $(\Delta I_{nterference}/\Delta I_{RBD}) \times 100$, where $\Delta I_{nterference}$ obtained from the change in current of interference at 0.1 ng/mL. The results indicated that the normalized current of MERS-CoV, RSV, Coxsackie, and Influenza were less than 5% compared with SARS-CoV-2, which means that the presence of these antigens does not affect to this immunosensor. However, the normalized current of SARS-CoV-1 was more than 5%. This means that N Protein SARS-CoV-1 does affect this proposed system. This reactivity can be explained by the similarity of structure and amino acid sequence of SARS-CoV-1 N protein compare to SARS-CoV-2 [39]. Therefore, N protein of SARS-CoV-1 is able to trigger immune responses against SARS-CoV-2 as well [40].

3.6. Reproducibility and stability of paper-based immunosensor

To demonstrate the reproducibility of the paper-based immunosensor, three electrodes were tasted with three different concentrations of SARS-CoV-2 spike protein RBD (0.01, 25, 100 ng/mL). The %RSD was obtained in the range of 0.3–2.9% (n = 3) which were less than 5%, indicating that this proposed immunosensor offers good reproducibility for the detection of SARS-CoV-2.

In order to evaluate the stability, the prepared immunosensor was stored in refrigerator at 4 °C before testing with 0.5 μg/mL RBD every 3 days. It was observed that 98.17% of its initial current response was retained within a storage lifetime of 5 days as shown in Fig. S3. The short lifetime of the proposed paper-based immunosensor might be affected by the humid condition during the storage.

3.7. Detection of SARS-CoV-2 in nasopharyngeal swab and throat swab samples

To illustrate the capability of the proposed system, the paper-based immunosensor was applied for detecting SAR-CoV-2 antigen in 14

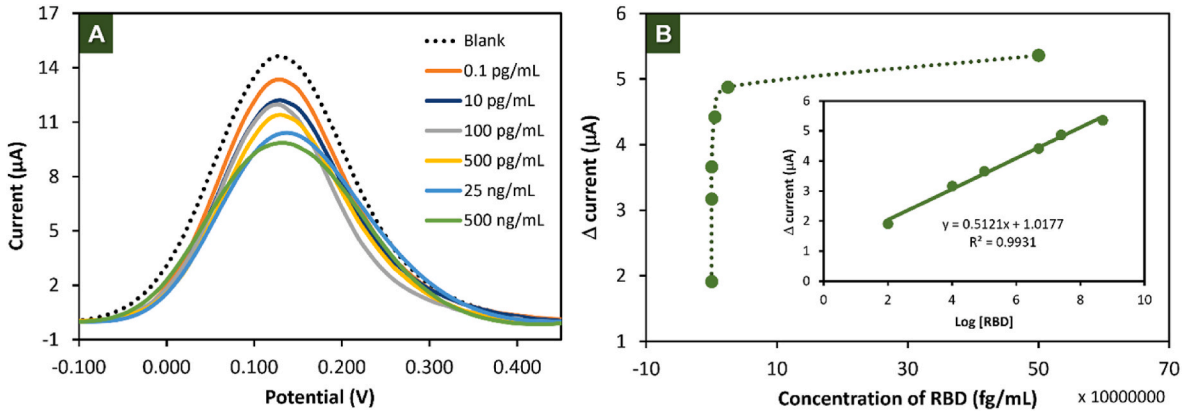

Fig. 3. (A) DPV response in 5 mM $[Fe(CN)_6]^{3-/4-}$ of the proposed immunosensor in different concentration of RBD in the range of 0.1 pg/mL to 500 ng/mL. (B) Relationship between Δ current and the concentration of RBD (inset is the calibration curve for proposed immunosensor).

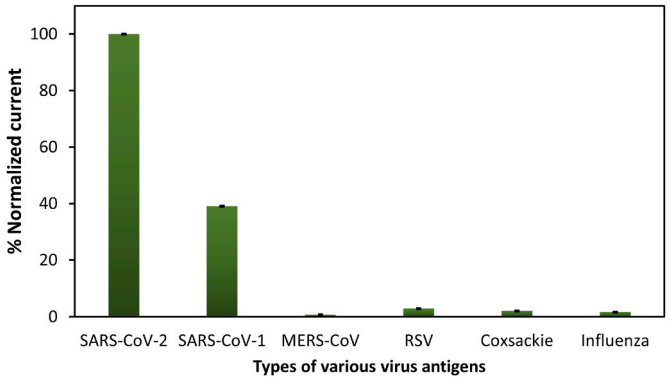

Fig. 4. Cross-reactivity of the proposed immunosensor.

nasopharyngeal swab and throat samples obtained from Ramathibodi hospital. All collected specimens were stored in viral transport media (VTM) solution at −80 °C prior to use without any dilution. The results obtained from our system were compared to those determined by RT-PCR standard method as summarized in Table 1. The good agreement between two approaches were observed, the sensitivity and specificity of our sensing system were found to be 100%. These results clearly showed that the paper-based immunosensor could be used for the screening of SARS-CoV-2 in real clinical samples. However, the plant-based monoclonal antibody CR3022 used in this work was designed to recognize the RBD of SARS-CoV-2 spike protein reference sequence Wuhan-Hu-1. The other SARS-CoV-2 variants could not be recognized by CR3022 since the amino acid residues in the SARS-CoV-2 spike protein have undergone mutations [41,42]. This alteration of spike structure would change in immune response in crucial epitopes recognized by mAb.

3.8. Determination of SARS-CoV-2 in saliva

To demonstrate that our approach can be extended to apply in various types of samples, the paper-based immunosensor was applied to detect SARS-CoV-2 in artificial saliva. The selectivity for saliva application was firstly examined. The proposed immunosensor was tested with various interferences that can be possibly found in saliva, including glucose, ascorbic acid (AA) and human serum albumin (HSA) [43,44]. All examined interferences were prepared by mixing with the SARS-CoV-2 RBD (0.5 μg/mL) in the concentration that was 100 times higher than target RBD. As shown in Fig. S4, the change in current response was identically observed on RBD relative to RBD mixed with other interferences (%RSD was less than 2%). This result indicated that the proposed immunosensor provided a good selectivity for screening of SARS-CoV-2 in saliva sample. The standard addition of artificial saliva containing varied SARS-CoV-2 concentrations was then studied. The concentration of RBD at 0.05, 1.0, 20 and 400 ng/mL were spiked into artificial saliva. According to Table S2, the percent recoveries of spiked RBD were obtained in an acceptable range from 40 to 120 with %RSD of 0.6–13.2 [45]. This result indicated that the paper-based immunosensor can be extended to detect SARS-CoV-2 in saliva sample.

Table 1
The comparison of obtained results between the proposed immunosensor and RT-PCR method.

		RT-PCR	
		+	−
This immunosensor	+	4	0
	−	0	10

+: positive result, −: negative result.

4. Conclusions

A novel electrochemical paper-based antigen sensing platform was successfully developed for detection of SARS-CoV-2. The electrochemical detection using DPV was performed based on a simple label-free immunoassay by measuring the current change via $[Fe(CN)_6]^{3-/4-}$ before and after addition of target RBD. The existing feature of our proposed system is the use of the innovative plant-based mAb CR3022 that provides a remarkable simplicity and cost-effectiveness in terms of Ab production. Moreover, the excellent sensitivity was achieved by taking the advantage of CNC as it offers the abundant sites of COOH functional group for Ab immobilization. The LOD and LOQ were found to be 2.0 fg/mL and 8.0 fg/mL with high specificity. The proposed sensing device was then applied with nasopharyngeal swab samples and the system showed 100% of sensitivity and specificity compared to standard RT-PCR method. Additionally, we also demonstrated that our existing system can be extended to detect SARS-CoV-2 RBD in saliva sample. Given the low-cost and high specificity of the antibody used, adaptability of the system towards different kind of samples, and the simplicity of use benefiting from the label-free assay, development of this approach provided a valuable alternative tool for rapid screening of COVID-19. While we are targeting SARS-CoV-2 with this platform, our device can be easily adapted towards other targets by switching the capture antibody, allowing this system to be utilized in various diagnostic applications.

Credit author statement

Jutamas Jaewjaroenwattana: Conceptualization, Methodology,

Investigation, Validation, Writing – original draft. **Waranyoo Phoolcharoen**: Resources, Writing – review & editing. **Ekawat Pasomsub**: Resources. **Prinjaporn Teengam**: Conceptualization, Methodology, Writing – review & editing. **Orawon Chailapakul**: Supervision, Project administration, Funding acquisition.

Declaration of competing interest

The authors declare that they have no known competing financial interests or personal relationships that could have appeared to influence the work reported in this paper.

Data availability

Data will be made available on request.

Acknowledgements

JJ acknowledges the funding from the 90th Anniversary of Chulalongkorn University Fund (GCUGR1125651046M). PT gratefully appreciates the support from the Second Century Fund (C2F), Chulalongkorn University. OC thanks financial support from National Research Council of Thailand (NRCT) (N35A640020). The authors would like to acknowledge the support from the Electrochemistry and Optical Spectroscopy Center of Excellence (EOSCE), Chulalongkorn University. The authors also thank Dr. Wisarut Khamcharoen for kindly assistance with manuscript editing.

Appendix A. Supplementary data

Supplementary data to this article can be found online at https://doi.org/10.1016/j.talanta.2022.123783.

References

[1] sprinklr, WHO coronavirus (COVID-19) dashboard. https://covid19.who.int, 2022. Accessed May 14 2022.
[2] D. Santoni, N. Ghosh, I. Saha, An entropy-based study on mutational trajectory of SARS-CoV-2 in India, Infection, Genet. Evol. 97 (2022), 105154.
[3] K.-J. Shan, C. Wei, Y. Wang, Q. Huan, W. Qian, Host-specific asymmetric accumulation of mutation types reveals that the origin of SARS-CoV-2 is consistent with a natural process, Innovation 2 (4) (2021), 100159.
[4] P.M. Etaware, Virtual system for early detection of COVID-19 infection "Etaware-CDT-2020 prototype design" (corroborated by rRT-PCR data), Biomed. Signal Process Control 73 (2022), 103337.
[5] H. García, A. Allende-López, P. Morales-Ruíz, G. Miranda-Novales, M.Á. Villasis-Keever, COVID-19 in neonates with positive RT–PCR test. Systematic review, Arch. Med. Res. 53 (3) (2022) 252–262.
[6] A.A. Alfadda, M. AlKhowaiter, N. Alotaibi, K. Alayed, M. Alzahrani, K. Binkhamis, K. Siddiqui, A. Youssef, H. Altalhi, I. Almaghlouth, M. Alarifi, S. Albanyan, M. F. Alosaimi, R. Hasanato, A. Isnani, H. Dekhil, M. Rafiullah, Clinical and biochemical characteristics and outcomes of suspected COVID-19 hospitalized patients: RT-PCR swab positive and negative comparison, J. Infect. Pub. Health 14 (11) (2021) 1623–1629.
[7] Y.-R. Jhou, C.-H. Wang, H.-P. Tsai, Y.-S. Shan, G.-B. Lee, An integrated microfluidic platform featuring real-time reverse transcription loop-mediated isothermal amplification for detection of COVID-19, Sensor. Actuator. B Chem. 358 (2022), 131447.
[8] A. Ge, F. Liu, X. Teng, C. Cui, F. Wu, W. Liu, Y. Liu, X. Chen, J. Xu, B. Ma, A Palm Germ-Radar (PaGeR) for rapid and simple COVID-19 detection by reverse transcription loop-mediated isothermal amplification (RT-LAMP), Biosens. Bioelectron. 200 (2022), 113925.
[9] H. Kitajima, Y. Tamura, H. Yoshida, H. Kinoshita, H. Katsuta, C. Matsui, A. Matsushita, T. Arai, S. Hashimoto, A. Iuchi, T. Hirashima, H. Morishita, H. Matsuoka, T. Tanaka, T. Nagai, Clinical COVID-19 diagnostic methods: comparison of reverse transcription loop-mediated isothermal amplification (RT-LAMP) and quantitative RT-PCR (qRT-PCR), J. Clin. Virol. 139 (2021), 104813.
[10] T. Mueller, Antibodies against severe acute respiratory syndrome coronavirus type 2 (SARS-CoV-2) in individuals with and without COVID-19 vaccination: a method comparison of two different commercially available serological assays from the same manufacturer, Clin. Chim. Acta 518 (2021) 9–16.
[11] M. Infantino, M. Pieri, M. Nuccetelli, V. Grossi, B. Lari, F. Tomassetti, G. Calugi, S. Pancani, M. Benucci, P. Casprini, M. Manfredi, S. Bernardini, The WHO International Standard for COVID-19 serological tests: towards harmonization of anti-spike assays, Int. Immunopharm. 100 (2021), 108095.
[12] A. Sakuraba, A. Luna, D. Micic, Serologic response to coronavirus disease 2019 (COVID-19) vaccination in patients with immune-mediated inflammatory diseases: a systematic review and meta-analysis, Gastroenterology 162 (1) (2022) 88–108, e9.
[13] Y. Li, V.M. Cassone, A simple, specific high-throughput enzyme-linked immunosorbent assay (ELISA) for quantitative determination of melatonin in cell culture medium, Int. Immunopharm. 28 (1) (2015) 230–234.
[14] S. Sakamoto, W. Putalun, S. Vimolmangkang, W. Phoolcharoen, Y. Shoyama, H. Tanaka, S. Morimoto, Enzyme-linked immunosorbent assay for the quantitative/qualitative analysis of plant secondary metabolites, J. Nat. Med. 72 (1) (2018) 32–42.
[15] J.-L. Wu, W.-P. Tseng, C.-H. Lin, T.-F. Lee, M.-Y. Chung, C.-H. Huang, S.-Y. Chen, P.-R. Hsueh, S.-C. Chen, Four point-of-care lateral flow immunoassays for diagnosis of COVID-19 and for assessing dynamics of antibody responses to SARS-CoV-2, J. Infect. 81 (3) (2020) 435–442.
[16] Y. Zhou, Y. Wu, L. Ding, X. Huang, Y. Xiong, Point-of-care COVID-19 diagnostics powered by lateral flow assay, TrAC, Trends Anal. Chem. 145 (2021), 116452.
[17] A. Somborac Bačura, M. Dorotić, L. Grošić, M. Džimbeg, S. Dodig, Current status of the lateral flow immunoassay for the detection of SARS-CoV-2 in nasopharyngeal swabs, Biochem. Med. 31 (2) (2021), 020601-020601.
[18] A. Yakoh, U. Pimpitak, S. Rengpipat, N. Hirankarn, O. Chailapakul, S. Chaiyo, Paper-based electrochemical biosensor for diagnosing COVID-19: detection of SARS-CoV-2 antibodies and antigen, Biosens. Bioelectron. 176 (2021), 112912.
[19] F.A. Azri, R. Sukor, J. Selamat, F. Abu Bakar, N.A. Yusof, R. Hajian, Electrochemical immunosensor for detection of aflatoxin B(1) based on indirect competitive ELISA, Toxins 10 (5) (2018).
[20] Z. Rahmati, M. Roushani, H. Hosseini, H. Choobin, An electrochemical immunosensor using SARS-CoV-2 spike protein-nickel hydroxide nanoparticles bioconjugate modified SPCE for ultrasensitive detection of SARS-CoV-2 antibodies, Microchem. J. 170 (2021), 106718.
[21] S. Boonkaew, P. Teengam, S. Jampasa, S. Rengpipat, W. Siangproh, O. Chailapakul, Cost-effective paper-based electrochemical immunosensor using a label-free assay for sensitive detection of ferritin, Analyst 145 (14) (2020) 5019–5026.
[22] N. Ruecha, K. Shin, O. Chailapakul, N. Rodthongkum, Label-free paper-based electrochemical impedance immunosensor for human interferon gamma detection, Sensor. Actuator. B Chem. 279 (2019) 298–304.
[23] Y. Fan, S. Shi, J. Ma, Y. Guo, A paper-based electrochemical immunosensor with reduced graphene oxide/thionine/gold nanoparticles nanocomposites modification for the detection of cancer antigen 125, Biosens. Bioelectron. 135 (2019) 1–7.
[24] E. Noviana, T. Ozer, C.S. Carrell, J.S. Link, C. McMahon, I. Jang, C.S. Henry, Microfluidic paper-based analytical devices: from design to applications, Chem. Rev. 121 (19) (2021) 11835–11885.
[25] T. Ozer, C.S. Henry, Paper-based analytical devices for virus detection: recent strategies for current and future pandemics, Trends Anal. Chem. 144 (2021), 116424.
[26] L.A. Mercante, A. Pavinatto, T.S. Pereira, F.L. Migliorini, D.M. dos Santos, D. S. Correa, Nanofibers interfaces for biosensing: design and applications, Sens. Act. Rep. 3 (2021), 100048.
[27] S. Palanisamy, S.K. Ramaraj, S.-M. Chen, T.C.K. Yang, P. Yi-Fan, T.-W. Chen, V. Velusamy, S. Selvam, A novel laccase biosensor based on laccase immobilized graphene-cellulose microfiber composite modified screen-printed carbon electrode for sensitive determination of catechol, Sci. Rep. 7 (2017), 41214-41214.
[28] M.U. Nessa, M.A. Rahman, Y. Kabir, Plant-produced monoclonal antibody as immunotherapy for cancer, BioMed Res. Int. 2020 (2020), 3038564-3038564.
[29] K. Rattanapisit, Z. Chao, K. Siriwattananon, Z. Huang, W. Phoolcharoen, Plant-produced anti-enterovirus 71 (EV71) monoclonal antibody efficiently protects mice against EV71 infection, Plants 8 (12) (2019).
[30] A.G. Diamos, J.G.L. Hunter, M.D. Pardhe, S.H. Rosenthal, H. Sun, B.C. Foster, M. P. DiPalma, Q. Chen, H.S. Mason, High level production of monoclonal antibodies using an optimized plant expression system, Front. Bioeng. Biotechnol. 7 (2019) 472.
[31] K. Rattanapisit, B. Shanmugaraj, S. Manopwisedjaroen, P.B. Purwono, K. Siriwattananon, N. Khorattanakulchai, O. Hanittinan, W. Boonyayothin, A. Thitithanyanont, D.R. Smith, W. Phoolcharoen, Rapid production of SARS-CoV-2 receptor binding domain (RBD) and spike specific monoclonal antibody CR3022 in Nicotiana benthamiana, Sci. Rep. 10 (1) (2020), 17698.
[32] K. Rattanapisit, T. Phakham, S. Buranapraditkun, K. Siriwattananon, C. Boonkrai, T. Pisitkun, N. Hirankarn, R. Strasser, Y. Abe, W. Phoolcharoen, Structural and in vitro functional analyses of novel plant-produced anti-human PD1 antibody, Sci. Rep. 9 (1) (2019), 15205.
[33] J.S. Park, H.J. Kim, J.H. Lee, J.H. Park, J. Kim, K.S. Hwang, B.C. Lee, Amyloid beta detection by faradaic electrochemical impedance spectroscopy using interdigitated microelectrodes, Sensors 18 (2) (2018).
[34] H. Zhao, F. Liu, W. Xie, T.-C. Zhou, J. OuYang, L. Jin, H. Li, C.-Y. Zhao, L. Zhang, J. Wei, Y.-P. Zhang, C.-P. Li, Ultrasensitive supersandwich-type electrochemical sensor for SARS-CoV-2 from the infected COVID-19 patients using a smartphone, Sensor. Actuator. B Chem. 327 (2021), 128899.
[35] F. Nan, Q. Chen, P. Liu, S. Nagarajan, Y. Duan, J. Zhang, Iridescent graphene/cellulose nanocrystal film with water response and highly electrical conductivity, RSC Adv. 6 (96) (2016) 93673–93679.
[36] S.D. Tallapragada, K. Layek, R. Mukherjee, K.K. Mistry, M. Ghosh, Development of screen-printed electrode based immunosensor for the detection of HER2 antigen in human serum samples, Bioelectrochemistry 118 (2017) 25–30.
[37] P. Pusomjit, P. Teengam, N. Thepsuparungsikul, S. Sanongkiet, O. Chailapakul, Impedimetric determination of cortisol using screen-printed electrode with aptamer-modified magnetic beads, Mikrochim. Acta 188 (2) (2021) 41.

[38] S. Jampasa, P. Lae-Ngee, K. Patarakul, N. Ngamrojanavanich, O. Chailapakul, N. Rodthongkum, Electrochemical immunosensor based on gold-labeled monoclonal anti-LipL32 for leptospirosis diagnosis, Biosens. Bioelectron. 142 (2019), 111539.
[39] T. Gao, M. Hu, X. Zhang, H. Li, L. Zhu, H. Liu, Q. Dong, Z. Zhang, Z. Wang, Y. Hu, Y. Fu, Y. Jin, K. Li, S. Zhao, Y. Xiao, S. Luo, L. Li, L. Zhao, J. Liu, H. Zhao, Y. Liu, W. Yang, J. Peng, X. Chen, P. Li, Y. Liu, Y. Xie, J. Song, L. Zhang, Q. Ma, X. Bian, W. Chen, X. Liu, Q. Mao, C. Cao, Highly pathogenic coronavirus N protein aggravates lung injury by MASP-2-mediated complement over-activation, medRxiv (2020), 2020.03.29.20041962.
[40] R. Gorkhali, P. Koirala, S. Rijal, A. Mainali, A. Baral, H.K. Bhattarai, Structure and function of major SARS-CoV-2 and SARS-CoV proteins, Bioinf. Biol. Insights 15 (2021), 11779322211025876.
[41] W.T. Harvey, A.M. Carabelli, B. Jackson, R.K. Gupta, E.C. Thomson, E.M. Harrison, C. Ludden, R. Reeve, A. Rambaut, C.-G.U. Consortium, S.J. Peacock, D. L. Robertson, SARS-CoV-2 variants, spike mutations and immune escape, Nat. Rev. Microbiol. 19 (7) (2021) 409–424.
[42] S.M. Hirabara, T.D.A. Serdan, R. Gorjao, L.N. Masi, T.C. Pithon-Curi, D.T. Covas, R. Curi, E.L. Durigon, SARS-COV-2 variants: differences and potential of immune evasion, Front. Cell. Infect. Microbiol. 11 (2021), 781429.
[43] J. Noiphung, M.P. Nguyen, C. Punyadeera, Y. Wan, W. Laiwattanapaisal, C. S. Henry, Development of paper-based analytical devices for minimizing the viscosity effect in human saliva, Theranostics 8 (14) (2018) 3797–3807.
[44] K. Kaewnu, K. Promsuwan, A. Phonchai, A. Thiangchanya, D. Somapa, N. Somapa, K. Tayayuth, W. Limbut, Cost-effective foam-based colorimetric sensor for roadside testing of alcohol in undiluted saliva, Chemosensors 9 (12) (2021).
[45] A. International, Guidelines for Standard Method Performance Requirements, 2016.